

# Facile Synthesis of a Crystalline Zinc Sulfide/Chitosan Biopolymer Nanocomposite: Characterization and Application for Photocatalytic Degradation of Textile Dyes and Anticancer Activity

Bilal Ahmad Bhat,\* Nimisha Jadon,\* Laxmi Dubey, and Showkat Ahmad Mir



Cite This: *ACS Omega* 2024, 9, 24425–24437



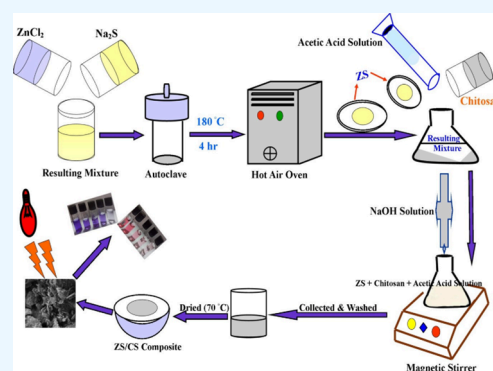
Read Online

ACCESS |

Metrics & More

Article Recommendations

**ABSTRACT:** In the present study, we have synthesized a zinc sulfide/chitosan (ZS/CS) nanocomposite by utilizing simple, economical, and environmentally friendly methods. The synthesized nanomaterials were characterized by different analytical techniques such as XRD, FE-SEM, EDS, and FTIR to determine the phase structure, morphology, and elemental composition. FTIR spectroscopy was used to confirm the functional groups of the synthesized zinc sulfide (ZS) nanoparticles and ZS/CS composite. Besides, the optical properties of the as-synthesized nanocomposite was analyzed by a UV–visible spectrophotometer, and the estimated band gap energy is  $\sim 3.03$  eV. The photocatalytic efficiency of the synthesized ZS/CS nanocomposite was investigated against two textile dyes, Crystal Violet (CV) and Acid Red-I (AR-I), under UV–visible light irradiation. The nanocomposite showed excellent photocatalytic activity against the dyes, and photodegradation was estimated to be about 93.44 and 90.67% for CV and AR-I, respectively. The nanocomposite was reused for three consecutive cycles. The results revealed that the photocatalyst displayed good reusability during the photocatalytic decomposition and thus is considered a cost-effective and promising photocatalyst in degrading dye pollutants. The kinetic study proved that the pseudo-first-order reaction kinetics was followed by the degradation process. We also examined the anticancer activity of ZS and ZS/CS against human breast and myelogenous leukemia cancer cell lines, namely, MCF-7 and K-562, and the half minimal inhibitory concentrations were found to be less than  $50 \mu\text{g/mL}$ .



## INTRODUCTION

Water is an essential requirement for the majority of biological and industrial processes. No creature can survive without water. Currently, access to potable water is a serious issue in most countries in the world. One of the major causes of this issue is water pollution by contaminants such as chemical fertilizers, pesticides, and organic textile dyes.<sup>1–3</sup> Many industries, especially paper, textile, leather, plastic, electroplating, food processing, pharmaceutical, and agricultural, have been mushroomed for fulfilling the demands of the ever-increasing population.<sup>4,5</sup> Although the textile industry is a major contributor to economic growth, it also produces a significant amount of textile wastes that are negatively affecting the environment.<sup>6,7</sup> The majority of textile industrial processes rely on organic dyes to color their products, which are subsequently released into freshwater reservoirs like rivers and streams that eventually flow into large water bodies like oceans.<sup>8,9</sup> Approximately, 20% of these industrial dyes are discharged into natural water bodies as effluents, thus affecting the aquatic ecosystems due to having nondestructive characteristics.<sup>10–12</sup> These dyes have the potential to reduce the penetration of sunlight into the aquatic systems, which may

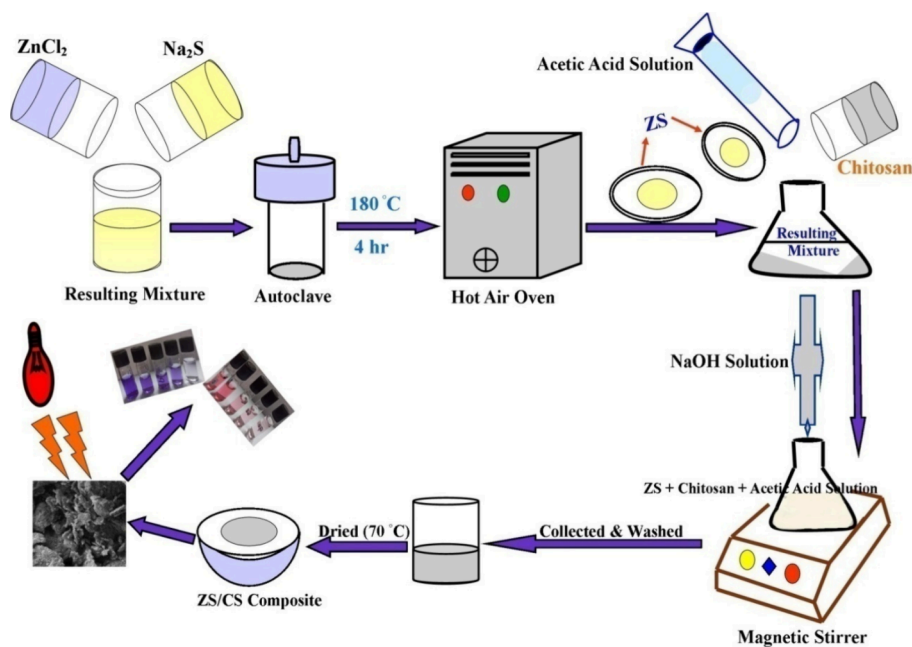
have an impact on the photosynthetic activity of aquatic flora and eventually disrupt the ecological food chains in aquatic ecosystems.<sup>13</sup> Among the hazardous dyes, Crystal Violet (a common triphenyl methane dye) and Acid Red -I (an aryl azo naphthol compound) are being used extensively in the textile industry, leather, or printing industry and are released in excess quantities with industrial effluents into aquatic systems. In addition, being toxic to mammalian cells, these can possibly act as powerful carcinogens, mutagens, and mitotic poisons when released in large amounts into the water bodies.<sup>14,15</sup>

To remove the aforementioned pollutants from wastewater or industrial effluents, a variety of conventional techniques have been adopted including adsorption, ultrafiltration, biodegradation, flocculation, electrochemical reduction, photocatalytic oxidation, reverse osmosis, and ion exchange.<sup>16–20</sup>

**Received:** January 8, 2024  
**Revised:** February 12, 2024  
**Accepted:** March 29, 2024  
**Published:** June 3, 2024



Scheme 1. Schematic Representation of the Synthesis and Application of the Catalyst



The creation of novel and advanced techniques for water treatment, which are essentially affordable, simple, secure, and environmentally friendly, is the only way to address the abovementioned environmental concern. By far the most efficient, affordable, and rapid way to break down organic pollutants is photocatalytic oxidation because it eliminates water contaminants by utilizing hydroxyl and other radical species.<sup>21</sup> Heterogeneous photocatalysts exploiting inorganic nanostructure metal chalcogenide semiconductors as photocatalysts are primarily used for environmental remediation owing to low cost, superior photostability, eco-friendliness, and ability to produce innocuous byproducts.<sup>22–24</sup>

A possible approach to improve the effectiveness of metal chalcogenides is to take advantage of biopolymers as a supporting substance. Biopolymers integrated with metallic nanoparticles are being used expansively as these biopolymers amplify the individual properties of the nanoparticles. Recently, there has been a large focus on the development of metal chalcogenides to be utilized as dye decomposition photocatalysts.<sup>25,26</sup> The utilization of polymers to provide stability, chemical consistency, and enhanced mechanical durability to nanoparticles has drawn attention to polymer-based photocatalysts, which combine the advantages of both nanoparticles and polymers.<sup>27–29</sup>

Chitosan, a well-known polysaccharide, is composed of D-glucosamine and N-acetyl-D-glucosamine connected by a  $\beta$ -1-4-glycosidic bond. Notably, chitosan is a flexible biopolymer that is derived from chitin by a process of alkaline deacetylation and can be used as a capping agent to stabilize and prepare nanocomposites.<sup>30,31</sup> Chitosan is rich with amine and hydroxyl groups, which facilitates possible chemical modification of the substance.<sup>32,33</sup> The reactive amine ( $-\text{NH}_2$ ) and hydroxyl (OH) groups in chitosan make it an effective sorbent for an array of organic pollutants.<sup>34–36</sup> Chitosan is well-known for having vast applications in biomedical, adsorption, purification, and the food packaging sector owing to its unique macromolecular structure, biological activity, biocompatibility, biodegradability, and other intrinsic

properties, due to which it has attained significant attention in recent scientific research.<sup>37–40</sup>

The aim of the present study is to synthesize a ZS/CS nanocomposite, to evaluate its effectiveness for photocatalytic decomposition of textile dyes from aqueous medium, and also to evaluate the anticancer activity of the synthesized nanocomposite. The synthesized materials were employed for different characterization techniques, such as XRD, SEM, EDS, FTIR, and UV–Vis spectroscopy. Furthermore, the photocatalytic dye decomposition efficiency of the prepared nanocomposite was evaluated against two textile dyes from aqueous medium. Crystal Violet (CV) and Acid Red-I (AR-I) are taken as model pollutant dyes in the present study. Langmuir–Hinshelwood kinetics was used to study the kinetic behavior of the photodegradation process. The anticancer potential of the synthesized samples (ZS and ZS/CS) was also assessed against human breast and myelogenous leukemia cancer cell lines. To the best of our knowledge, a zinc sulfide/chitosan composite has not been reported in the literature for the photocatalytic degradation of Crystal violet and Acid Red-I dyes and for anticancer activity. In this study, we synthesized the composite in a short duration of time as compared with already reported works. The graphical representation of the synthesis and application is shown in Scheme 1.

## ■ MATERIALS AND METHODS

For the synthesis of materials, analytical reagent (AR) grade chemicals were used as supplied by CDH, RANKEM. The chemicals used for this research work were zinc chloride ( $\text{ZnCl}_2$ ; purity >98%), sodium sulfide ( $\text{Na}_2\text{S}$ ; purity 98%), sodium hydroxide pellets (NaOH; purity >97%), acetic acid ( $\text{CH}_3\text{COOH}$ ; purity >98%), chitosan (extracted from shrimp shells with 75% degree of deacetylation), Crystal Violet and Acid Red-I dyes, trichloroacetic acid (30%), and sulforhodamine B (SRB). The whole experiment was conducted with double distilled water.

**Synthesis of Zinc Sulfide.** The zinc sulfide nanostructures were synthesized by a simple and inexpensive hydrothermal

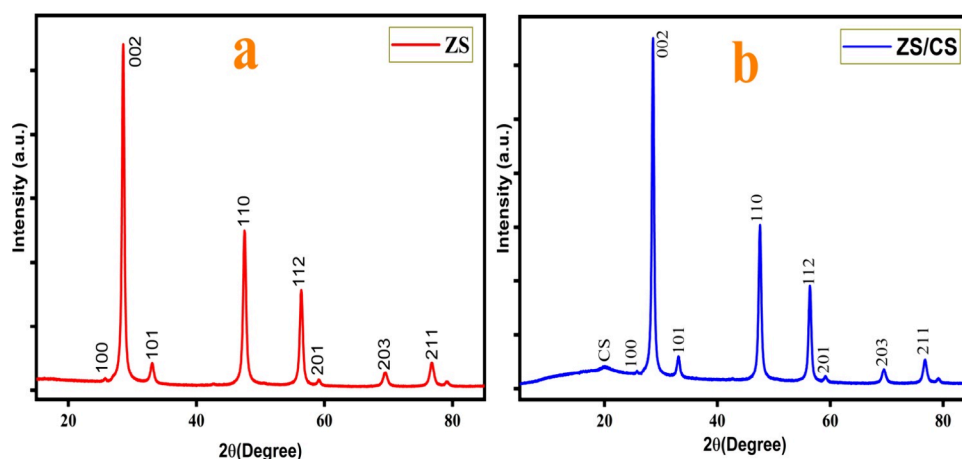


Figure 1. XRD diffraction patterns of (a) ZS and (b) ZS/CS.

route using  $\text{ZnCl}_2$  and  $\text{Na}_2\text{S}$  as precursor salts in 1:1 molar ratio, by adopting the methodology used in previous works by Assadullah et al.<sup>41</sup> Briefly, 25 mL of sodium sulfide and 25 mL of zinc chloride solution were mixed by continuous stirring for 40 min at room temperature. Subsequently, the resulting white gel was loaded into a 60 mL stainless-steel autoclave with Teflon lining, and the autoclave was put inside a hot air oven at 180 °C for 4 h. After that, the autoclave was taken out from the oven and allowed to cool naturally to room temperature. The obtained white deposit was filtered using Whatman filter paper, washed several times with double distilled water, and finally dried at 70 °C in a hot air oven. The sample was stored in a glass vial and kept in a desiccator for further use, and the sample was named as ZS.

**Zinc Sulfide/Chitosan Composite.** The previously reported methodology with slight modification was adopted for the synthesis of the zinc sulfide/chitosan composite.<sup>42,43</sup> Briefly, 0.25g of ZS and 0.25g of chitosan were incorporated into 62 mL of 1.045 M acetic acid solution. After that, the solution mixture was agitated on a magnetic stirrer for 3 h. Further, 125 mL of 0.65 M NaOH solution was added slowly into this solution while stirring for an extra 3 h to precipitate the zinc sulfide/chitosan composite. Finally, the prepared whitish composite of zinc sulfide/chitosan was separated and washed thoroughly with double distilled water until neutral pH and kept in a hot air oven for drying at 70 °C. The dried sample was stored in an airtight vial for further use and characterization, and the sample was named as ZS/CS.

**Photocatalytic Activity.** The photocatalytic degradation of Crystal Violet and Acid Red-I dyes was examined by using the synthesized ZS/CS composite as a photocatalyst. To carry out the photocatalytic experiment, 50 mL of Crystal Violet and Acid Red-I dye solutions each of 20 mg/L dye concentration were prepared; then, 30 mg of ZS/CS nanocomposite was added to each solution. The experiment was performed under a UV–visible light source by using a high-pressure mercury lamp (Philips 70 W). Before exposure to UV–visible light, the dye solutions with a known amount of photocatalyst were magnetically stirred under darkness for 40 min to attain the adsorption/desorption equilibrium. Then, after subjecting to UV–visible light irradiation, small aliquots of sample were taken at regular intervals and centrifuged to separate the photocatalyst, and then, the absorbance of dye solution was determined using a UV–visible spectrophotometer. The degradation percentage of dyes was calculated by using eq 1<sup>44</sup>

$$\text{degradation efficiency (\%)} = \frac{A_0 - A_t}{A_0} \times 100 \quad (1)$$

where  $A_0$  is the initial absorbance of dye solution and  $A_t$  is the final absorbance after time  $t$ .

**In Vitro Cell Proliferation Assay.** The human breast and myelogenous leukemia cancer cell lines, namely, MCF-7 and K-562, were cultured in 96-well plates to evaluate the antiproliferative activity of ZS and ZS/CS in comparison to the positive control doxorubicin, following a previously established protocol.<sup>45</sup> The cell lines were obtained from the National Centre for Cell Sciences, Pune, Maharashtra, India. For each well,  $5 \times 10^3$  cells were seeded in a complete DMEM (Dulbecco's Modified Eagle Medium) medium and incubated for 24 h. Subsequently, the cells were exposed to 6.25, 12.5, 25, 50, 100, and 200  $\mu\text{g}/\text{mL}$  concentrations of ZS, ZS/CS, and doxorubicin for an additional 48 h incubation period under 5%  $\text{CO}_2$  and humid conditions. After the treatment, the cells were fixed using 30% trichloroacetic acid and stained with 0.4% sulforhodamine B (SRB). Unbound dye was removed by washing with 1% acetic acid, and the protein-bound dye was extracted with 10 mM Tris base. The absorbance of the plates was measured using a SPECTRAMax PLUS 384 microplate spectrophotometer. To determine the  $\text{IC}_{50}$  value, representing the concentration required to inhibit 50% of cell proliferation, a Quest Graph™  $\text{IC}_{50}$  Calculator online tool (AAT Bioquest, Inc., Sunnyvale, CA, <https://www.aatbio.com/tools/ic50-calculator>) was employed. The experimental procedure was conducted in triplicate to ensure robustness and reliability of the results.

**Characterization.** Several analytical techniques were employed to ascertain the structural, morphological, compositional, and optical characteristics of the prepared nanostructures. An XRD analytical technique (XRD, Rigaku Miniflex 600 with  $\text{Cu-K}\alpha$  radiation) was used to investigate the crystallite size and crystallinity of the synthesized ZS nanoparticles and ZS/CS composite. A PerkinElmer FT-IR spectrometer operating in the 4000–400  $\text{cm}^{-1}$  range was used for determining the functional groups of the synthesized samples. Elemental composition and surface morphology of the ZS nanoparticles and ZS/CS nanocomposite were investigated by using a FE-SEM (Philips Model-Quanta 200 FEG). A UV–Visible spectrophotometer (DB-20S Systronics-double beam) was employed to examine the optical properties of the synthesized samples. It was also used to determine the

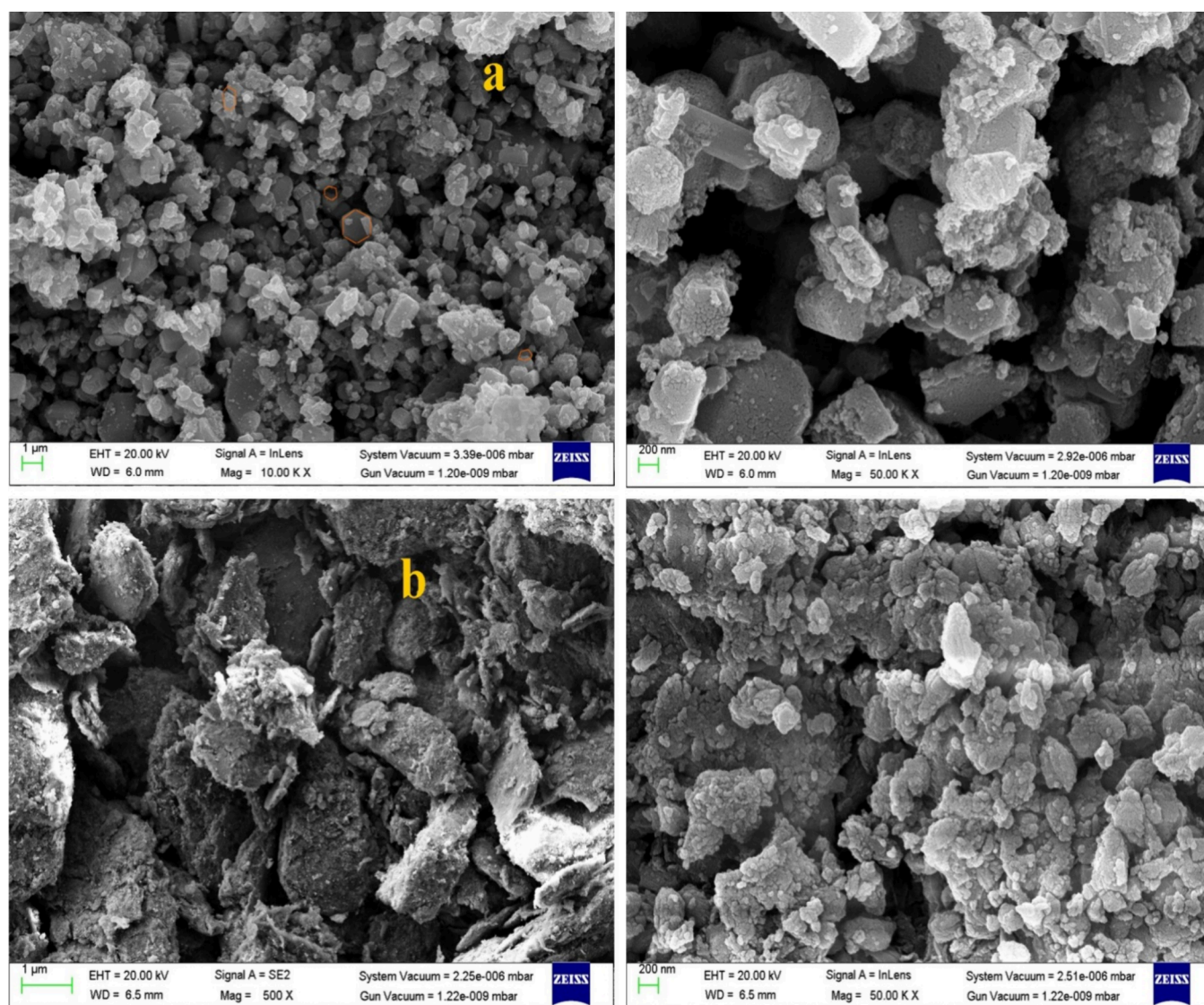


**Figure 2.** SEM images of the synthesized samples: (a) ZS and (b) ZS/CS.

absorbance of the dyes before and after illumination to find out the photocatalytic degradation.

## RESULTS AND DISCUSSION

**XRD.** X-ray diffraction (XRD) is a nondestructive analytical tool that provides comprehensive details about the crystallographic structure and phase-related properties of the prepared materials. Figure 1a,b illustrates the typical XRD spectra of ZS and the chitosan-zinc sulfide nanocomposite. The diffraction peaks on the ZS/CS nanocomposite reflect that it is composed of a hexagonal structural phase of zinc sulfide and well matched with the standard JCPDS data card no. 36-1450.<sup>46</sup> The diffraction spectra peaks are centered at  $2\theta$  values of  $\sim 26.11$ ,  $28.76$ ,  $31.01$ ,  $47.54$ ,  $56.40$ ,  $59.30$ ,  $69.51$ , and  $76.75^\circ$  that correspond to the reflections from the (100), (002), (101), (110) (112), (201), (203), and (211) crystal planes, respectively. The results are fairly consistent with those of previously reported studies.<sup>38,47–49</sup> The diffraction pattern shows no peaks corresponding to other phases or impurities, indicating that the prepared nanostructure is pure and devoid of any impurities. From Figure 2b, it is evident that the emergence of the chitosan XRD peak at  $2\theta = 20.03^\circ$  provides

evidence of the successful zinc sulfide/chitosan composite formation.<sup>50</sup> Using the Debye–Scherrer formula, as indicated in eq 2, the mean crystallite size of the synthesized ZS and ZS/CS nanocomposite was estimated from the high intensity peaks and calculated to be  $\sim 19.08$  and  $14.78$  nm, respectively.

$$D = \frac{k\lambda}{\beta \cos \theta} \quad (2)$$

where  $D$  denotes the average crystallite size of the nanostructure;  $k$  denotes a constant (0.9);  $\lambda$  is the X-ray wavelength;  $\beta$  represents the full width at half-maximum (fwhm), and  $\theta$  signifies Bragg's angle.

**SEM.** The surface morphology of the synthesized ZS and ZS-chitosan composite was examined by using the FE-SEM image, as displayed in Figure 2. The results show that the ZS samples are composed of hexagonal structures with some irregular shapes (Figure 2a). The SEM image of the ZS/CS composite is depicted in Figure 2b. It illustrates that the nanocomposite is flaky and has irregular and rough shape. The morphological changes verify that a composite has formed, which confirms the integration chitosan and zinc sulfide in the synthesized nanostructure.<sup>8</sup> Both samples exhibit anisotropic

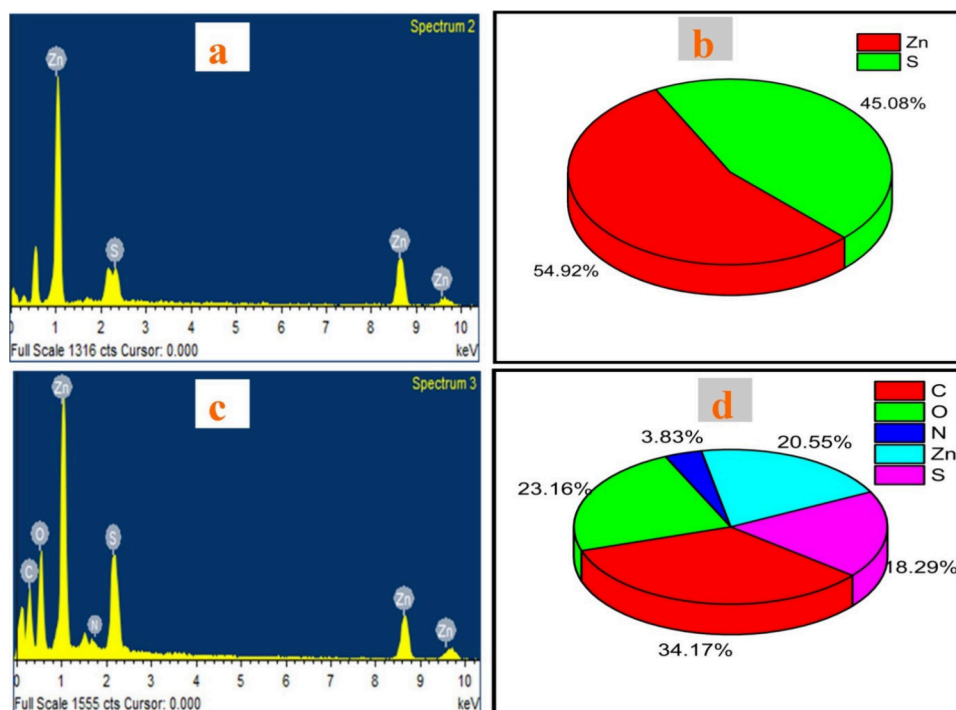


Figure 3. EDS spectrum of the synthesized samples (a) ZS and (c) ZS/CS and (b, d) their corresponding atomic percentage composition.

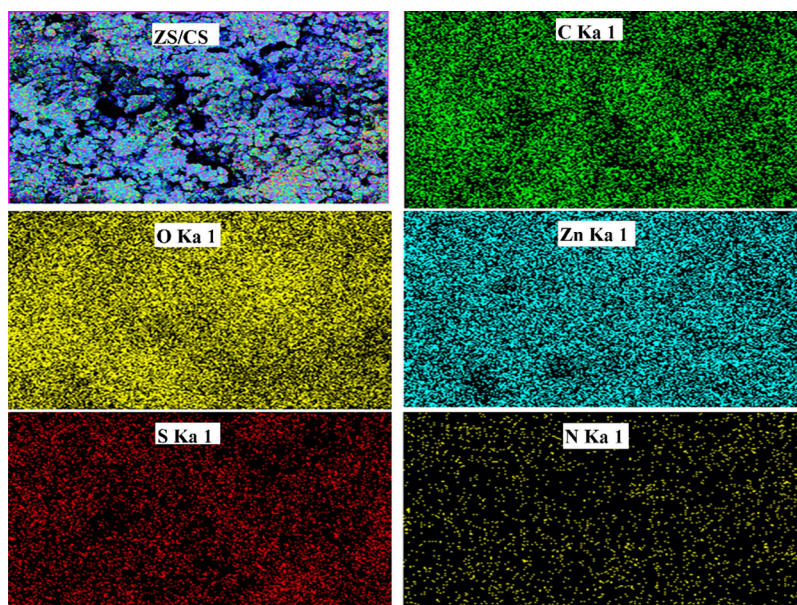


Figure 4. Elemental mapping of C, O, Zn, S, and N of sample ZS/CS.

growth that is attributed to the reaction medium (distilled water) used in the synthesis process. Autogeneous pressure that develops within the Teflon vessel during the hydrothermal process minimizes the viscosity of water and promotes ion mobility in the medium. Thus, higher reaction rates are favored, and this promotes anisotropic growth, leading to such morphology. Besides, growth is encouraged along specific facets because they are energetically efficient.<sup>51</sup> This is also evident from the XRD spectrum that illustrates higher diffraction peak intensity along the (002) peak than other peaks, suggesting a preferred growth direction along this axis.<sup>46</sup>

**EDS.** Energy-dispersive spectroscopy (EDS) of the as-synthesized materials was assessed to confirm our XRD results

and to ascertain material purity and successful synthesis. Besides, the elemental composition of the prepared samples is provided by the EDS study. The chosen areas of the SEM image provided the elemental analysis. The presence of zinc, sulfur, carbon, and oxygen elements in the EDS spectra of ZS and the ZS/CS composite shown in Figure 3a,c, respectively, validates the effective synthesis of ZS and the ZS/CS nanocomposite. The spectrum shows no additional peaks attributed to any element, indicating that the desired material was successfully prepared. Figure 3b,d shows the respective atomic percentage pie chart of ZS/and ZS/CS. The elemental distribution in the pure and composite nanomaterial was investigated by EDS mapping. The excellent preparation of the

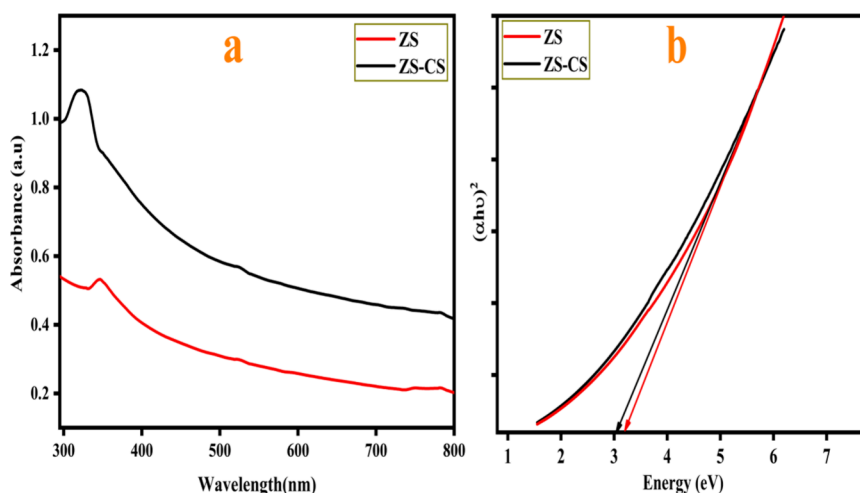


Figure 5. (a) Absorbance spectra and (b) band gap plot of the samples.

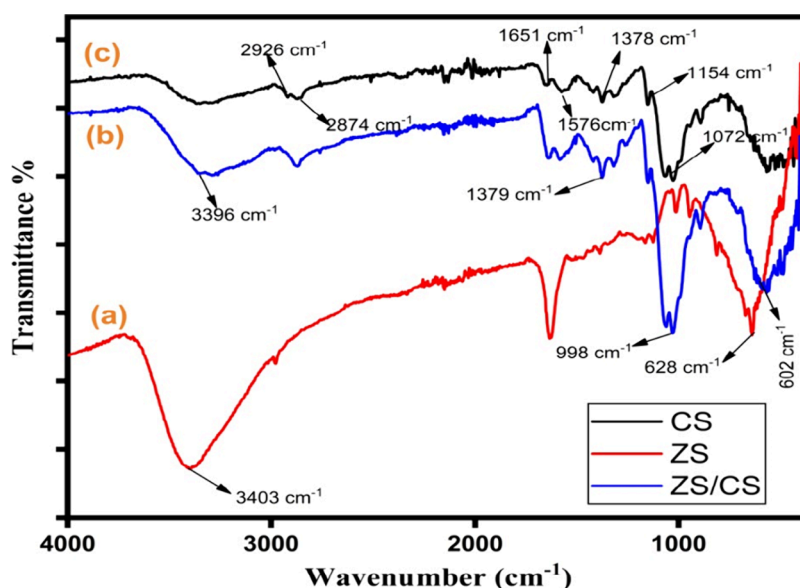


Figure 6. FT-IR spectrum of ZS (a), ZS/CS (b), and Chitosan (c).

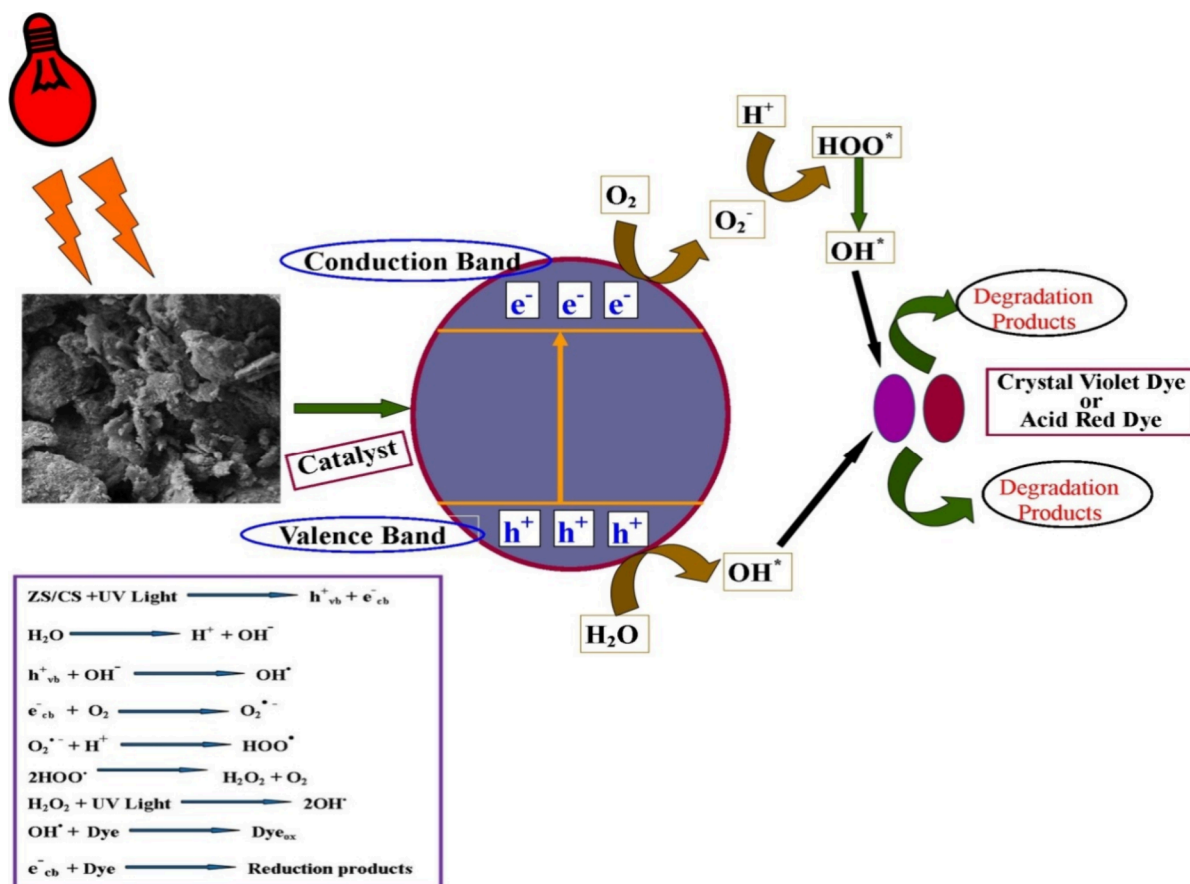
samples is suggested by the fairly homogeneous elemental distribution across all samples, as depicted in Figure 4, which is highlighted by different colors.

**Optical Properties.** UV–visible spectrophotometry was used for determining the optical properties of the synthesized samples. The synthesized ZS and ZS/CS composite were dispersed in isopropanol and kept on an ultrasonicator for 20 min to prepare a homogeneous solution. Then, absorption spectrum was recorded by scanning the samples between 200 and 800 nm wavelength ranges. Using a Tauc plot [ $(\alpha h\nu)^2$  vs  $h\nu$  ( $E_g$ )], the band gap values of the synthesized ZS and ZS/CS nanocomposite were determined by plotting the tangent line and the value was recorded where it intersects the  $x$ -axis ( $E_g$ ). Figure 5a,b depicts the absorbance spectrum and the respective band gap energy plot of the samples. The band gap energy values are estimated to be about 3.17 and 3.06 eV for ZS and ZS/CS samples, respectively. The results are in good agreement with previously reported works.<sup>52–54</sup> The absorption spectrum indicates that, in comparison to pure zinc sulfide, the composite sample has shown an increase in absorption intensity throughout the whole visible region.

Consequently, the ZS/CS composite has illustrated a smaller band gap value than the pure sample, which can lead to effective utilization of UV–visible light during the photocatalytic process.

**FTIR.** The FTIR spectra of ZS, CS, and the ZS/CS nanocomposite biopolymer were compared with the available data in the literature to support the successful synthesis of the composite. The bands that appeared at 628 and 996  $\text{cm}^{-1}$  are due to the zinc–sulfur bond’s stretching vibrations,<sup>38</sup> as shown in Figure 6a. The stretching vibrations that were detected at 3403  $\text{cm}^{-1}$  are characteristics of adsorbed water molecules.<sup>55</sup> The IR spectra of chitosan and the synthesized composite are displayed in Figure 6b,c. To verify the successful synthesis of the ZS/CS composite, it was compared with the previously reported FTIR spectra of the synthesized chitosan composite. The presence of Zn–S bond stretching vibrations was indicated by the characteristic bands at 602 and 998  $\text{cm}^{-1}$  in the FTIR spectrum of the fabricated ZS/CS composite. The results are in good agreement with the findings published in the literature.<sup>8,56</sup> The bands that appear at 1651  $\text{cm}^{-1}$  are caused by the C=O stretching modes that originate from an

Scheme 2. Graphical Representation of the Photocatalytic Degradation Mechanism



acetylated group of chitosan, while the broader band at  $3397\text{ cm}^{-1}$  is owing to the O–H stretch in chitosan that can also overlap with the possible N–H stretch.<sup>57,58</sup> The band that arises at  $1379\text{ cm}^{-1}$  is attributed to distortion of the  $CH_3$  group in the chitosan biopolymer.<sup>59,60</sup> Therefore, the results of FTIR obtained in our work are consistent with those of other reported studies related to the synthesis of a chitosan composite.

**Photocatalysis.** The use of semiconductor materials in photocatalytic degradation is primarily suggested for water treatment objectives owing to their high efficiency, photostability, environmentally friendly process, and ability to produce harmless byproducts.<sup>61,62</sup> The photocatalysis mechanism is depicted in Scheme 2.<sup>63,64</sup> If the synthesized photocatalyst composite is illuminated by a UV–visible light source, transition of electrons to a conduction band from the valence band occurs to generate an electron–hole pair. These active species lead to the formation of reactive  $OH^\bullet$  radicals and  $O_2^{\bullet -}$  anion radicals due to the redox reaction. The  $O_2^{\bullet -}$  anions further interact with  $H^+$  to form superoxide radicals. The superoxide radicals ( $HOO^\bullet$ ) along with  $OH^\bullet$  radicals cause the degradation of dye pollutants into nonpoisonous degradation products.<sup>65</sup> In the present study, the dye solutions were exposed to a light source, and then, sample aliquots were taken at regular intervals to record the absorbance spectra on the UV–vis spectrophotometer. Figure 7 and Figure 8 depict the absorbance versus illumination time for CV and AR-I dye solutions, respectively. CV shows a major absorption peak at  $\lambda = 582\text{ nm}$  and AR-I at  $530\text{ nm}$ . According to the Lambert–Beer law, a drop in absorbance with increasing irradiation time

denotes a decrease in dye concentrations and consequently their degradation.<sup>66</sup> It was determined that the prepared catalyst degraded  $\sim 93.44\%$  of CV in 120 min, whereas AR dye was degraded to  $90.67\%$  upon illumination by a light source. The results of photocatalytic decomposition show that CV shows a higher degradation percentage than AR-I dye. It is thought that the reason for this variation in degradation percentages is due to the nature of the dyes that were used. The cationic CV dye appears to be adsorbed over the negatively charged catalyst surfaces rapidly due to electrostatic interactions. The catalyst surfaces are believed to have negative charge due to the attached  $OH^-$  ions.<sup>67,68</sup> When the catalyst is illuminated, electrons from the valence band move into the conduction band, creating electron hole pairs. The more potent hydroxyl free radicals ( $OH^\bullet$ ) are produced when the holes are taken up by adsorbed hydroxyl ions. However, it is thought that  $O_2$  is converted into superoxides due to extraction of the electrons in the conduction band, which then react with water to produce more hydroxyl free radicals. These hydroxyl free radicals are believed to be the reasons for the efficient degradation of the CV dye by the ZS/CS composite. Since AR-I is an anionic dye, the adsorption of  $OH^-$  ions and consequently the generation of  $OH^\bullet$  free radicals are thought to occur at a very slower pace because of electrostatic repulsions between the negatively charged catalyst surfaces and the dye molecules.<sup>66</sup> Thus, a lesser degradation percentage is observed in the case of AR-I dye for the same extent of irradiation time. The degradation efficiency of the synthesized catalyst was calculated by the equation given below:

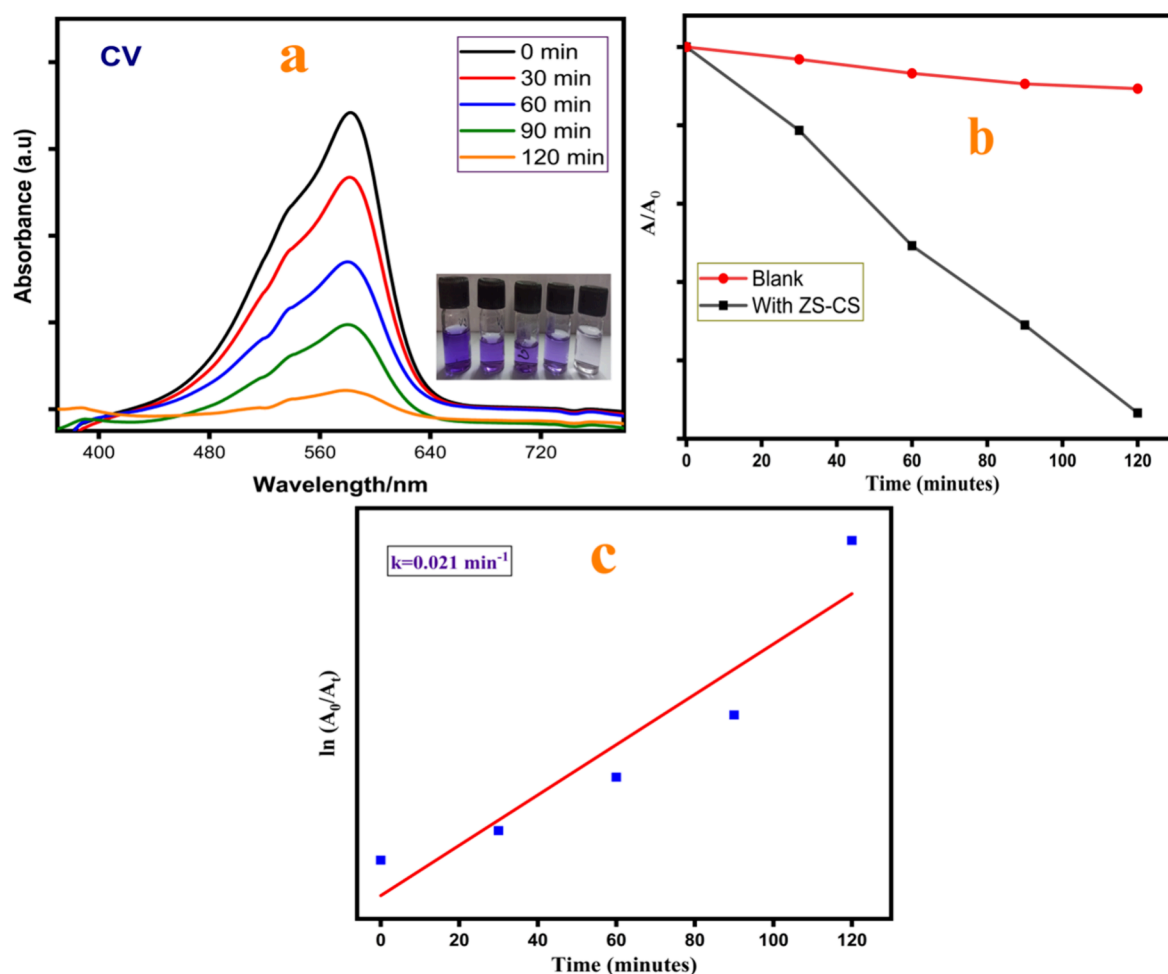


**Figure 7.** (a) Time-dependent absorbance spectra of CV treated with ZS/CS, (b) concentration curves of blank (without a catalyst) and with the synthesized composite, and (c) pseudo-first-order kinetic plot of photocatalytic degradation of CV dye.

$$\text{degradation efficiency (\%)} = \frac{A_0 - A_t}{A_0} \times 100$$

where  $A_0$  is the initial absorbance of dye solution and  $A_t$  is the final absorbance after time “ $t$ ”.

**Kinetics of the Photocatalytic Degradation.** Photocatalytic degradation of CV and AR-I was also studied to evaluate the kinetic behavior using Langmuir–Hinshelwood kinetic equation (eq 3)<sup>69–71</sup>

$$\ln\left(\frac{A_0}{A_t}\right) = kt \quad (3)$$

where  $A_0$  is the initial absorbance,  $A_t$  is the absorbance at time “ $t$ ”,  $k$  is the kinetics reaction rate constant, and  $t$  is the irradiation time. The photocatalytic decomposition of CV and AR-I dyes using the as-synthesized biopolymer composite followed the pseudo first-order kinetics as confirmed from the linear nature of the graphs shown in Figure 7c and Figure 8c, respectively. The estimated values of the rate constant ( $k$ ) and  $R^2$  (correlation coefficient) for CV and AR-I are given in Table 1.

The synthesized photocatalyst is of practical significance only when it is reused, is regenerated, and has high stability during photocatalysis. The synthesized ZS/CS was used for three successive cycles of photocatalysis degradation. To reuse the photocatalyst nanocomposite, the ZS/CS nano-

composite particles were separated by a centrifuge, washed thoroughly with double distilled water, and dried in a hot air oven. It was observed that the degradation efficiency drops from 93.44 to 87.64% (CV) and 90.67 to 84.37% (AR-I) even after the third cycle (Figure 9a). This indicates the catalyst’s capacity for reuse and confirms its high stability and its proficiency was maintained with a small reduction in degradation percentage.

To ascertain the role of active species ( $\text{OH}^\bullet$  radicals and superoxides) in the photocatalytic degradation of CV and AR, scavenging experiments were performed to utilize IPA (isopropyl alcohol) and AA (ascorbic acid) as scavengers of hydroxyl radicals and superoxides, respectively. As shown in Figure 9b, the bar diagrams illustrate the percentage of photodegradation in the presence and absence of scavengers. It is clearly visible from the bar graphs that the photodegradation process declines in the presence of both scavengers. Although bar diagrams show that the addition of scavengers reduces the photodegradation process, the addition of IPA as an  $\text{OH}^\bullet$  radical scavenger has substantially lowered the percentage of photodegradation, indicating that  $\text{OH}^\bullet$  radicals are crucial for the photocatalytic degradation of dyes. Therefore, it is proposed that active species generated during the photocatalytic process are responsible for the photodegradation, which is consistent with the mechanism of photodegradation reported in the previous literature.<sup>72,73</sup>

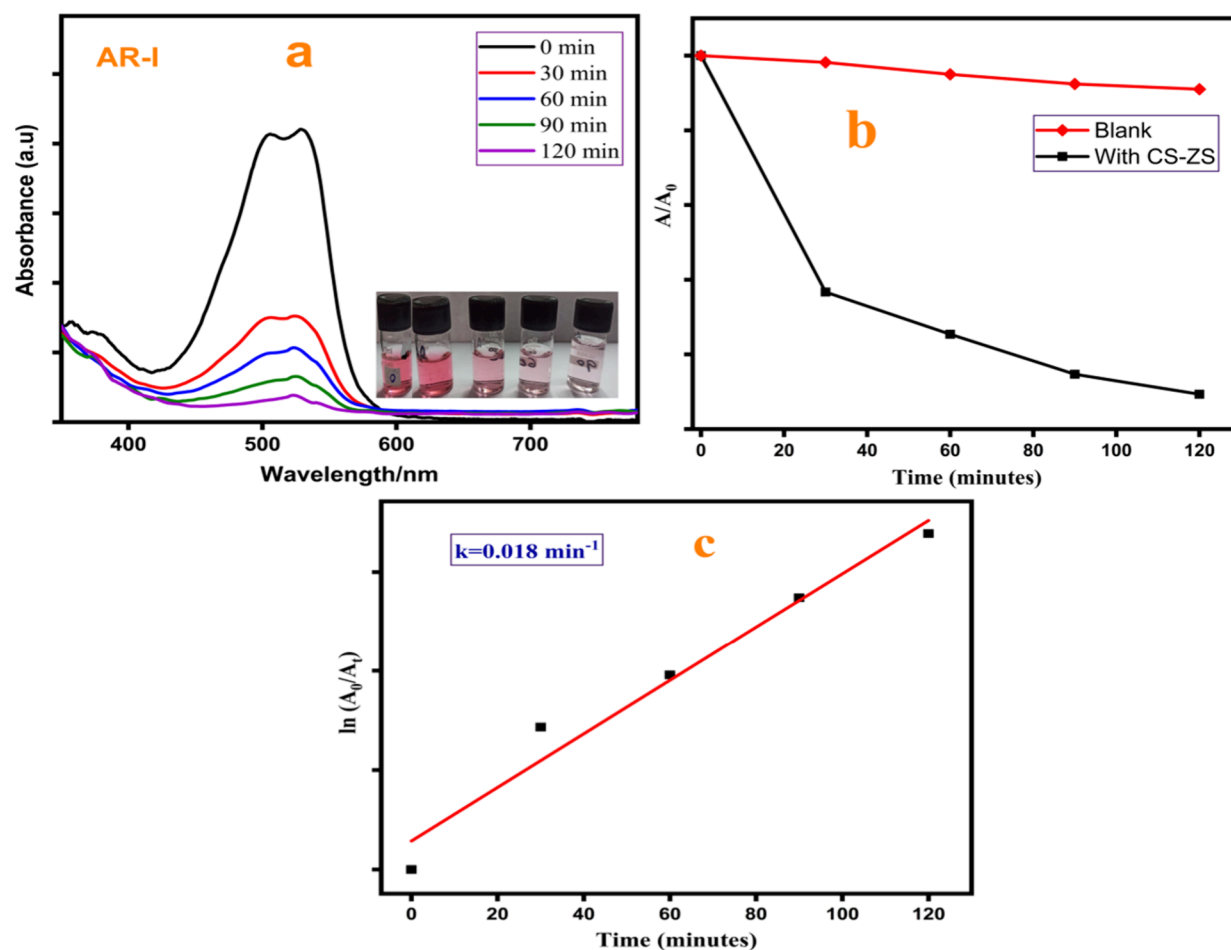


**Figure 8.** (a) Time-dependent absorbance spectra of AR-I treated with ZS/CS, (b) concentration curves of blank (without a catalyst) and with the synthesized composite, and (c) pseudo-first-order kinetic plot of photocatalytic degradation of AR-I dye.

**Table 1. Kinetics Rate Constant Value**

dye solution	$k$ ( $\text{min}^{-1}$ )	$R^2$
Crystal violet	0.021	0.901
Acid Red-I	0.018	0.968

To elucidate the practical application of the ZS/CS photocatalyst, we have carried out photodegradation of a mixture of CV + AR dye solution by using ZS/CS as a photocatalyst. The time-dependent absorption spectra obtained are shown in Figure 9c. The absorbance spectra consist of peaks belonging to CV (582 nm) as well as AR (~530 nm) whose amplitudes progressively fall under UV light illumination, hence confirming the photodegradation of the mixture of dye solution (Figure 9c). Therefore, the significant degradation shown by the photocatalyst against the mixture of dye solution validates its potential for practical wastewater treatments.

**Antiproliferative Activities of ZS, ZS/CS, and Doxorubicin.** We have examined the antiproliferative activities of the synthesized samples on breast cancer cell lines and myelogenous leukemia, namely, MCF-7 and K-562. By determining the  $IC_{50}$  values for ZS, ZS/CS, and doxorubicin in these cell lines, we obtained valuable insights into their respective potency and efficacy. The compiled  $IC_{50}$  values are graphically depicted in Figure 10 and Figure 11, underscoring the variability observed among myelogenous leukemia and breast cancer cell types and indicating a cell type-dependent

response to the compounds. In evaluating the inhibitory effect of ZS, ZS/CS, and doxorubicin on different cancer cell lines, compelling findings have emerged. When ZS/CS and ZS were used against the MCF-7 cancer cell line, the  $IC_{50}$  values were determined to be  $48.2 \pm 0.5$  and  $47.08 \pm 0.8$   $\mu\text{g}/\text{mL}$ . On the other hand, doxorubicin exhibited an  $IC_{50}$  value of  $2.5 \pm 0.6$   $\mu\text{g}/\text{mL}$  on the same cell line.

Furthermore, the application of ZS/CS and ZS to the K-562 cell line resulted in  $IC_{50}$  values of  $47.6 \pm 0.8$  and  $49.6 \pm 0.7$   $\mu\text{g}/\text{mL}$ , respectively, while doxorubicin displayed an  $IC_{50}$  value of  $3.2 \pm 0.5$   $\mu\text{g}/\text{mL}$ . These findings provide intriguing insights into the inhibitory potency of both ZS/CS and ZS, and doxorubicin was taken as a reference drug against these specific cancer cell lines. While definitive conclusions regarding the susceptibility of cancer cells to ZS/CS, ZS, and doxorubicin cannot be drawn solely based on these findings, it is evident that the mechanisms of cell death represent potential targets for the therapeutic effects of these drugs. Further investigations are warranted to elucidate the specific molecular pathways and signaling cascades affected by ZS/CS, ZS, and doxorubicin, providing deeper insights into their antiproliferative effects in myelogenous leukemia and breast cancer cell lines. Such investigations will contribute to our understanding of the underlying mechanisms and potentially pave the way for the development of novel therapeutic strategies targeting myelogenous leukemia and breast cancer cell lines.

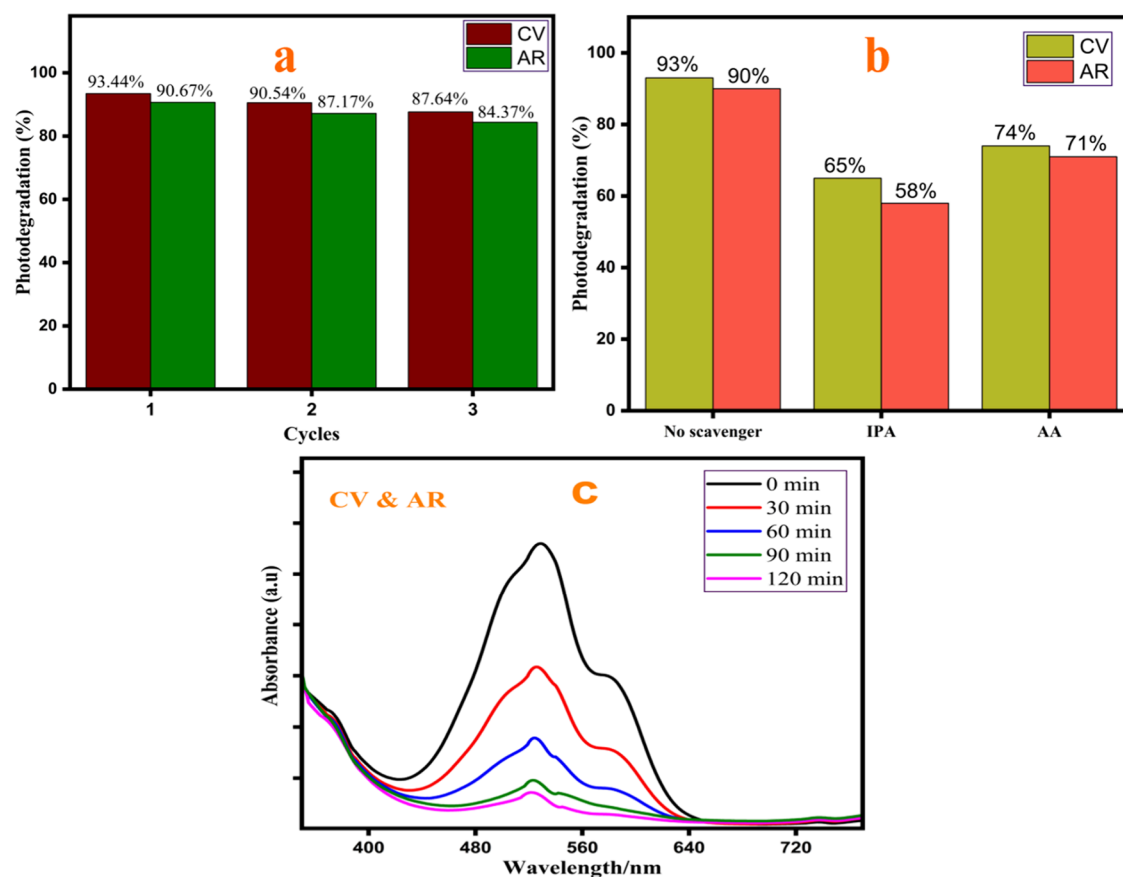


**Figure 9.** (a) Degradation percentages for three consecutive degradation cycles. (b) Degradation percentage in the absence and presence of scavengers. (c) Time-dependent absorbance spectra of a mixture of CV and AR-I dye solution treated with ZS/CS.

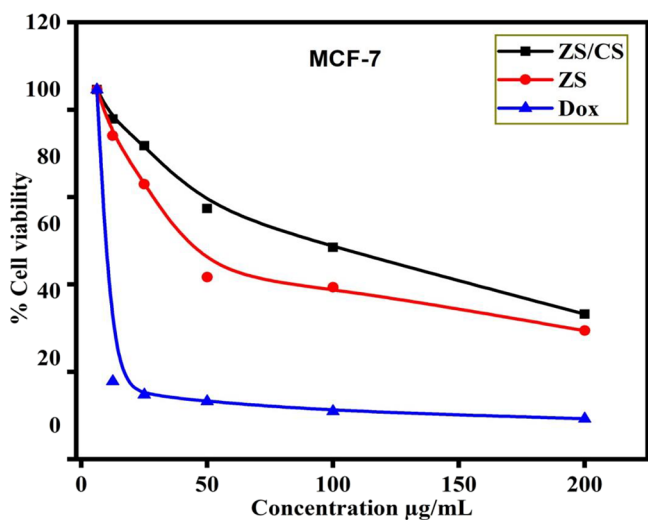


**Figure 10.** Concentration-dependent anticancer activity of ZS, ZS/CS, and doxorubicin against MCF-7 cell lines.

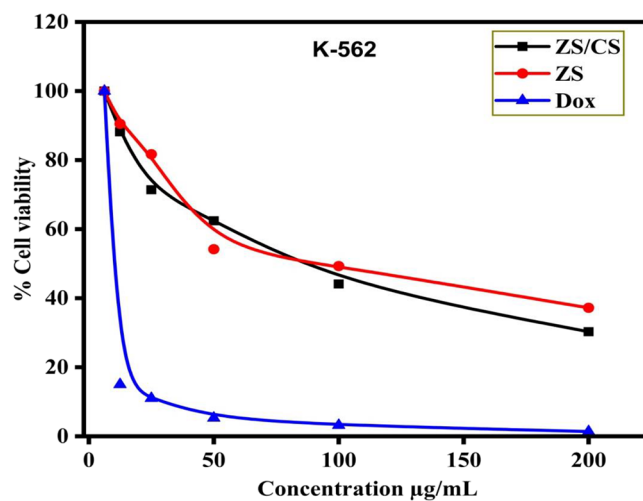


**Figure 11.** Concentration-dependent anticancer activity of ZS, ZS/CS, and doxorubicin against K-562 cell lines.

## CONCLUSIONS

In this study, we have synthesized zinc sulfide/chitosan biopolymer nanocomposite using facile and inexpensive hydrothermal and coprecipitation methods. The synthesized nanocomposite was characterized by different characterization tools such as XRD, FE-SEM, EDS, FTIR spectroscopy, and UV-vis spectroscopy. XRD analysis has shown the growth of

crystalline and hexagonal phase structures of the ZS/CS nanocomposite. The morphological studies have revealed the formation of irregular shapes of the biopolymer nanocomposite. Elemental-dispersive spectroscopy analysis of the synthesized nanocomposite confirmed its purity. The photocatalytic activity of the ZS/CS composite against two model dye pollutants, namely, CV and AR-I, has shown degradation effectiveness of 93.44 and 90.67%, respectively, under UV-visible light illumination. The degradation process of CV and

AR-I dye using the synthesized catalyst fitted well with the pseudo-first-order reaction kinetics with the rate constants 0.021 and 0.018 min<sup>-1</sup>, respectively. The synthesized ZS/CS composite exhibited excellent photocatalytic decomposition for both dyes as well as reusability for three consecutive cycles. Hence, the synthesized composite could be used as a promising catalyst for degradation of textile dye pollutants from aqueous environments. We also evaluated the anticancer activity of the synthesized ZS and ZS/CS samples against the MCF-7 and K-562 cancer cell lines. The findings of this study provide intriguing insights into the inhibitory potency of both ZS/CS and ZS samples. These synthesized samples in the present study exhibit noticeable activity on cancer cell lines and hence could be used for biomedical uses.

## AUTHOR INFORMATION

### Corresponding Authors

**Bilal Ahmad Bhat** – School of Studies in Environmental Science (IGAERE), Jiwaji University, Gwalior 474011, India; [orcid.org/0009-0006-9876-7913](https://orcid.org/0009-0006-9876-7913);  
Email: [bhatbilal787@gmail.com](mailto:bhatbilal787@gmail.com)

**Nimisha Jadon** – School of Studies in Environmental Chemistry, Jiwaji University, Gwalior 474011, India;  
Email: [nimisha09@yahoo.com](mailto:nimisha09@yahoo.com)

### Authors

**Laxmi Dubey** – Department of Botany, SMS, Govt. Model Science College, Gwalior 474009, India

**Showkat Ahmad Mir** – School of Life Sciences, Sambalpur University, Burla, Odisha 768019, India; [orcid.org/0000-0002-3668-2184](https://orcid.org/0000-0002-3668-2184)

Complete contact information is available at:  
<https://pubs.acs.org/10.1021/acsomega.4c00247>

### Author Contributions

**Bilal Ahmad Bhat**: Conceptualization, methodology, investigation, data analysis, writing - original draft. **Nimisha Jadon**: Conceptualization, supervision, validation, writing - review & editing. **Laxmi Dubey**: Visualization, validation, writing - review & editing. **Showkat Ahmad Mir**: Anticancer activity.

### Funding

This work is not funded by any agency.

### Notes

The authors declare no competing financial interest.

## ACKNOWLEDGMENTS

We are thankful to IIC-IIT Roorkee for providing the FESEM/EDS facility. We are also grateful to the CIF (Jiwaji University) for providing XRD and FTIR facilities. We also express our gratitude toward Dr. Dinesh of Advanced Environmental Testing & Research Lab Gwalior for providing the facility of UV-visible spectroscopy. We are also grateful to Rajesh Kumar Meher of School of Life Sciences, Sambalpur University, Odisha, for providing valuable support in analyzing the anticancer activity of this study.

## REFERENCES

- (1) Ren, D.; Yang, Y.; Yang, Y.; Richards, K.; Zhou, X. Land-Water-Food Nexus and indications of crop adjustment for water shortage solution. *Sci. Total Environ.* **2018**, *626*, 11–21.
- (2) Zheng, S.; Du, H.; Yang, L.; Tan, M.; Li, N.; Fu, Y.; Hao, D.; Wang, Q. PDINH bridged NH<sub>2</sub>-UiO-66 (Zr) Z-scheme hetero-

junction for promoted photocatalytic Cr (VI) reduction and antibacterial activity. *J. Hazard. Mater.* **2023**, *447*, No. 130849.

- (3) Dihom, H. R.; Al-Shaibani, M. M.; Mohamed, R. M. S. R.; Al-Gheethi, A. A.; Sharma, A.; Khamidun, M. H. B. Photocatalytic degradation of disperse azo dyes in textile wastewater using green zinc oxide nanoparticles synthesized in plant extract: A critical review. *J. Water Process Eng.* **2022**, *47*, No. 102705.

- (4) Ali, N.; Bilal, M.; Khan, A.; Ali, F.; Iqbal, H. M. Effective exploitation of anionic, nonionic, and nanoparticle-stabilized surfactant foams for petroleum hydrocarbon contaminated soil remediation. *Sci. Total Environ.* **2020**, *704*, No. 135391.

- (5) Ahmad, I.; Khan, S. B.; Kamal, T.; Asiri, A. M. Visible light activated degradation of organic pollutants using zinc-iron selenide. *J. Mol. Liq.* **2017**, *229*, 429–435.

- (6) Manikandan, V.; Elancheran, R.; Revathi, P.; Suganya, P.; Krishnasamy, K. Efficient photocatalytic degradation of crystal violet by using graphene oxide/nickel sulphide nanocomposites. *Bull. Mater. Sci.* **2020**, *43*, 1–10.

- (7) Cook, T. R.; Dogutan, D. K.; Reece, S. Y.; Surendranath, Y.; Teets, T. S.; Nocera, D. G. Solar energy supply and storage for the legacy and nonlegacy worlds. *Chem. Rev.* **2010**, *110* (11), 6474–6502.

- (8) Aziz, A.; Ali, N.; Khan, A.; Bilal, M.; Malik, S.; Ali, N.; Khan, H. Chitosan-zinc sulfide nanoparticles, characterization and their photocatalytic degradation efficiency for azo dyes. *Int. J. Biol. Macromol.* **2020**, *153*, 502–512.

- (9) Chong, M. N.; Jin, B.; Chow, C. W.; Saint, C. Recent developments in photocatalytic water treatment technology: a review. *Water research* **2010**, *44* (10), 2997–3027.

- (10) Ali, N.; Bilal, M.; Nazir, M. S.; Khan, A.; Ali, F.; Iqbal, H. M. N. Thermochemical and electrochemical aspects of carbon dioxide methanation: A sustainable approach to generate fuel via waste to energy theme. *Sci. Total Environ.* **2020**, *712*, No. 136482.

- (11) Sharma, H. K.; Ahmad, B.; Sofi, I. R.; Rambaboo. A Study of Starch Nanomaterial as Adsorbent in Removal of Heavy Metals from Aqueous Medium. *J. Environ. Res. Dev.* **2019**, *13* (3), 226–235.

- (12) Mugumo, R.; Tichapondwa, S. M.; Chirwa, E. M. N. Photocatalytic Degradation of Rhodamine B using CuS-doped ZnS under Visible Light Irradiation. *Chem. Eng. Trans.* **2022**, *94*, 1447–1452.

- (13) Nasirian, M.; Mehrvar, M. Photocatalytic degradation of aqueous Methyl Orange using nitrogen-doped TiO<sub>2</sub> photocatalyst prepared by novel method of ultraviolet-assisted thermal synthesis. *Journal of Environmental Sciences* **2018**, *66*, 81–93.

- (14) Patil, R.; Zahid, M.; Govindwar, S.; Khandare, R.; Vyavahare, G.; Gurav, R.; Desai, N. & Jadhav, J. (2022). Constructed wetland: A promising technology for the treatment of hazardous textile dyes and effluent. In *Development in Wastewater Treatment Research and Processes* (pp 173–198). Elsevier.

- (15) Al-Tohamy, R.; Ali, S. S.; Li, F.; Okasha, K. M.; Mahmoud, Y. A. G.; Elsamahy, T.; Jiao, H.; Fu, Y.; Sun, J. A critical review on the treatment of dye-containing wastewater: Ecotoxicological and health concerns of textile dyes and possible remediation approaches for environmental safety. *Ecotoxicol. Environ. Saf.* **2022**, *231*, No. 113160.

- (16) Cinperi, N. C.; Ozturk, E.; Yigit, N. O.; Kitis, M. Treatment of woolen textile wastewater using membrane bioreactor, nanofiltration and reverse osmosis for reuse in production processes. *Journal of cleaner production* **2019**, *223*, 837–848.

- (17) Wang, S.; Wang, Z.; Wang, Y.; Xia, C.; Hong, E.; Bai, L.; Li, T.; Wang, B. Study on the controlled synthesis and photocatalytic performance of rare earth Nd deposited on mesoporous TiO<sub>2</sub> photocatalysts. *Sci. Total Environ.* **2019**, *652*, 85–92.

- (18) Gui, L.; Peng, J.; Li, P.; Peng, R.; Yu, P.; Luo, Y. Electrochemical degradation of dye on TiO<sub>2</sub> nanotube array constructed anode. *Chemosphere* **2019**, *235*, 1189–1196.

- (19) Khan, A.; Ali, N.; Bilal, M.; Malik, S.; Badshah, S.; Iqbal, H. M. N. Engineering functionalized chitosan-based sorbent material: characterization and sorption of toxic elements. *Appl. Sci.* **2019**, *9* (23), 5138.

- (20) Xiao, X.; Li, T. T.; Lu, X. R.; Feng, X. L.; Han, X.; Li, W. W.; Li, Q.; Yu, H. Q. A simple method for assaying anaerobic biodegradation of dyes. *Bioresour. Technol.* **2018**, *251*, 204–209.
- (21) Sartaj, S.; Ali, N.; Khan, A.; Malik, S.; Bilal, M.; Khan, M.; Ali, N.; Hussain, S.; Khan, H.; Khan, S. Performance evaluation of photolytic and electrochemical oxidation processes for enhanced degradation of food dyes laden wastewater. *Water Sci. Technol.* **2020**, *81* (5), 971–984.
- (22) Abdullah, D.; Gupta, D. C. Scrutinizing the structural, optoelectronic, mechanical, and thermoelectric properties of semiconductor lead-free double perovskites  $A_2AgMoBr_6$  ( $A = K, Rb, Cs$ ). *Opt. Quantum Electron.* **2023**, *55*, 1277.
- (23) Lone, M. A.; Shrotriya, V.; Lone, T. A.; Alshahrani, T.; Hossain, M. A.; Adam, M.; Zaman, M. B. Rapid hydrothermal synthesis of mesoporous NiS<sub>2</sub> and NiSe<sub>2</sub> nanostructures for wastewater treatment. *Heliyon* **2023**, *9* (12), e22308 DOI: 10.1016/j.heliyon.2023.e22308.
- (24) Xu, J.; Lu, L.; Zhu, C.; Fang, Q.; Liu, R.; Wang, D.; He, Z.; Song, S.; Shen, Y. Insights into conduction band flexibility induced by spin polarization in titanium-based metal–organic frameworks for photocatalytic water splitting and pollutants degradation. *J. Colloid Interface Sci.* **2023**, *630*, 430–442.
- (25) Zaman, M. B.; Poolla, R.; Khandy, S. A.; Modi, A.; Tiwari, R. K. Thioglycolic acid assisted hydrothermal growth of SnS 2D nanosheets as catalysts for photodegradation of industrial dyes. *Nanotechnology* **2021**, *32* (24), 245706.
- (26) Khan, H.; Khalil, A. K.; Khan, A. Photocatalytic degradation of alizarin yellow in aqueous medium and real samples using chitosan conjugated tin magnetic nanocomposites. *J. Mater. Sci.: Mater. Electron.* **2019**, *30*, 21332–21342.
- (27) Sharma, M. V.; Sharma, H. K. Application of Polypyrrole/Lead Sulphide Nanocomposite in UV Light Assisted Photocatalysis and Gas Sensing. *J. Polym. Compos.* **2021**, *9*, 13–27.
- (28) Sharma, M. V.; Sharma, H. K.; Jadon, N. A study on degradation of methyl orange under UV light irradiation and ammonia gas sensing by polypyrrole/lead selenide nanocomposite. *Adv. Bio. Res.* **2021**, *12*, 1–12.
- (29) Franco, P.; Sacco, O.; De Marco, I.; Vaiano, V. Zinc oxide nanoparticles obtained by supercritical antisolvent precipitation for the photocatalytic degradation of crystal violet dye. *Catalysts* **2019**, *9* (4), 346.
- (30) Govindan, S.; Nivethaa, E. A. K.; Saravanan, R.; Narayanan, V.; Stephen, A. Synthesis and characterization of chitosan–silver nanocomposite. *Applied Nanoscience* **2012**, *2*, 299–303.
- (31) Zhang, Y.; Zhou, L.; Han, B.; Li, W.; Li, B.; Zhu, L. Research Progress of Chitosan Supported Copper Catalyst in Organic Reactions. *Chin. J. Org. Chem.* **2022**, *42* (1), 33.
- (32) Kusriani, E.; Wilson, L. D.; Padmosoedarso, K. M.; Mawarni, D. P.; Sufyan, M.; Usman, A. Synthesis of Chitosan Capped Zinc Sulphide Nanoparticle Composites as an Antibacterial Agent for Liquid Handwash Disinfectant Applications. *Journal of Composites Science* **2023**, *7* (2), 52.
- (33) Lim, M. J.; Shahri, N. N. M.; Taha, H.; Mahadi, A. H.; Kusriani, E.; Lim, J. W.; Usman, A. Biocompatible chitin-encapsulated CdS quantum dots: Fabrication and antibacterial screening. *Carbohydr. Polym.* **2021**, *260*, No. 117806.
- (34) Ali, N.; Khan, A.; Bilal, M.; Malik, S.; Badshah, S.; Iqbal, H. M. N. Chitosan-based bio-composite modified with thiocarbamate moiety for decontamination of cations from the aqueous media. *Molecules* **2020**, *25* (1), 226–238.
- (35) Zimet, P.; Mombrú, Á. W.; Mombrú, D.; Castro, A.; Villanueva, J. P.; Pardo, H.; Rufo, C. Physico-chemical and antilisterial properties of nisin-incorporated chitosan/carboxymethyl chitosan films. *Carbohydr. Polym.* **2019**, *219*, 334–343.
- (36) Khan, A.; Badshah, S.; Airoidi, C. Biosorption of some toxic metal ions by chitosan modified with glycidylmethacrylate and diethylenetriamine. *Chem. Eng. J.* **2011**, *171* (1), 159–166.
- (37) Jadon, N.; Bhat, G. A.; Sharma, M. V.; Sharma, H. K. Photocatalytic Degradation of Methyl Orange Dye with Synthesized Chitosan/Fe<sub>2</sub>O<sub>3</sub> Nanocomposite and its Isotherm Studies. *Current Nanoscience* **2022**, *18* (1), 78–85.
- (38) Xaba, T. Green synthesis of ZnS nanoparticles and fabrication of ZnS–chitosan nanocomposites for the removal of Cr(vi) ion from wastewater. *Green Processing and Synthesis* **2021**, *10* (1), 374–383.
- (39) Jadon, N.; Sharma, H. K. PANI/chitosan/ionic liquid/GCE sensor for the selective quantification of domperidone (DMP) and pantoprazole (PTZ). *Analytical Chemistry Letters* **2020**, *10* (4), 537–549.
- (40) Khan, S. B.; Ali, F.; Kamal, T.; Anwar, Y.; Asiri, A. M.; Seo, J. CuO embedded chitosan spheres as antibacterial adsorbent for dyes. *Int. J. Biol. Macromol.* **2016**, *88*, 113–119.
- (41) Assadullah, I.; Malik, J. H.; Shafi, A.; Tomar, R. Growth of crystalline WO<sub>3</sub>-ZnSe nanocomposites: an approach to optical, electrochemical, and catalytic properties. *Sci. Rep.* **2022**, *12* (1), 3962.
- (42) Khan, A.; Shah, S. J.; Mehmood, K.; Awais Ali, N.; Khan, H. Synthesis of potent chitosan beads a suitable alternative for textile dye reduction in sunlight. *J. Mater. Sci.: Mater. Electron.* **2019**, *30*, 406–414.
- (43) Abdelrahman, E. A.; Hegazey, R. M. Utilization of waste aluminum cans in the fabrication of hydroxysodalite nanoparticles and their chitosan biopolymer composites for the removal of Ni (II) and Pb (II) ions from aqueous solutions: kinetic, equilibrium, and reusability studies. *Microchem. J.* **2019**, *145*, 18–25.
- (44) Qin, S.; Liu, Y.; Zhou, Y.; Chai, T.; Guo, J. Synthesis and photochemical performance of CdS nanoparticles photocatalysts for photodegradation of organic dye. *Journal of Materials Science: Materials in Electronics* **2017**, *28*, 7609–7614.
- (45) Mir, S. A.; Mohanta, P. P.; Meher, R. K.; Baitharu, I.; Behera, A. K.; Raut, S.; Nayak, B. Bioinspired thiazolo-[2, 3-b] quinazolin-6-one derivatives as potent anti-cancer agents targeting EGFR: their biological evaluations and in silico assessment. *Mol. Diversity* **2023**, *1*–16.
- (46) Gawai, U. P.; Deshpande, U. P.; Dole, B. N. A study on the synthesis, longitudinal optical phonon–plasmon coupling and electronic structure of Al doped ZnS nanorods. *RSC Adv.* **2017**, *7* (20), 12382–12390.
- (47) Mustafa, H. N.; Al-Ogaidi, I. Efficacy of zinc sulfide-chitosan nanoparticles against bacterial diabetic wound infection. *Iraqi J. Agric. Sci.* **2023**, *54* (1), 1–17.
- (48) Munyai, S.; Mahlaule-Glory, L. M.; Hintsho-Mbita, N. C. Green synthesis of Zinc sulphide (ZnS) nanostructures using *S. frutescences* plant extract for photocatalytic degradation of dyes and antibiotics. *Materials Research Express* **2022**, *9* (1), No. 015001.
- (49) Zhao, J. G.; Zhang, H. H. Hydrothermal synthesis and characterization of ZnS hierarchical microspheres. *Superlattices Microstruct.* **2012**, *51* (5), 663–667.
- (50) Abdelrahman, E. A.; Hegazey, R. M. Exploitation of Egyptian insecticide cans in the fabrication of Si/Fe nanostructures and their chitosan polymer composites for the removal of Ni (II), Cu (II), and Zn (II) ions from aqueous solutions. *Composites Part B* **2019**, *166*, 382–400.
- (51) Malik, K. A.; Tomar, R.; Malik, J. H.; Zaman, M. B. One pot synthesis of ZnO hexagonal bugle beads in a closed polypropylene vessel: a simple hydrothermal way of synthesizing nanocrystalline ZnO photocatalyst for waste water treatments. *Nano Express* **2020**, *1* (1), No. 010010.
- (52) Alharbi, A.; Shah, R. K.; Sayqal, A.; Subaihi, A.; Alluhaybi, A. A.; Algethami, F. K.; Naglah, A. M.; Almezahia, A. A.; Katouah, H. A.; Youssef, H. M. Facile synthesis of novel zinc sulfide/chitosan composite for efficient photocatalytic degradation of acid brown 5G and acid black 2BNG dyes. *Alexandria Eng. J.* **2021**, *60* (2), 2167–2178.
- (53) Caires, A. J.; Mansur, A. A.; Carvalho, I. C.; Carvalho, S. M.; Mansur, H. S. Green synthesis of ZnS quantum dot/biopolymer photoluminescent nanopores for bioimaging brain cancer cells. *Mater. Chem. Phys.* **2020**, *244*, No. 122716.

- (54) Kaur, J.; Gupta, A.; Pandey, O. P. Photocatalytic study of ZnS-Ag<sub>2</sub>S nanocomposites-effect of thioglycerol. *Sol. Energy* **2018**, *176*, 678–687.
- (55) Liu, L. N.; Dai, J. G.; Zhao, T. J.; Guo, S. Y.; Hou, D. S.; Zhang, P.; Shang, J.; Wang, S.; Han, S. A novel Zn (ii) dithiocarbamate/ZnS nanocomposite for highly efficient Cr<sup>6+</sup> removal from aqueous solutions. *RSC Adv.* **2017**, *7* (56), 35075–35085.
- (56) Rema Devi, B. S.; Raveendran, R.; Vaidyan, A. V. Synthesis and characterization of Mn<sup>2+</sup>-doped ZnS nanoparticles. *Pramana* **2007**, *68* (4), 679–687.
- (57) Senapati, U. S.; Sarkar, D. Structural, spectral and electrical properties of green synthesized ZnS nanoparticles using *Elaeocarpus floribundus* leaf extract. *Journal of Materials Science: Materials in Electronics* **2015**, *26*, 5783–5791.
- (58) Khan, A.; Badshah, S.; Airoldi, C. Dithiocarbamated chitosan as a potent biopolymer for toxic cation remediation. *Colloids Surf., B* **2011**, *87* (1), 88–95.
- (59) Khan, A.; Begum, S.; Ali, N.; Khan, S.; Hussain, S.; Sotomayor, M. D. P. T. Preparation of crosslinked chitosan magnetic membrane for cations sorption from aqueous solution. *Water Sci. Technol.* **2017**, *75* (9), 2034–2046.
- (60) Iranmanesh, P.; Saeednia, S.; Nourzpoor, M. Characterization of ZnS nanoparticles synthesized by co-precipitation method. *Chinese Physics B* **2015**, *24* (4), No. 046104.
- (61) Nassar, M. Y.; Ali, A. A.; Amin, A. S. A facile Pechini sol-gel synthesis of TiO<sub>2</sub>/Zn<sub>2</sub> TiO<sub>2</sub>/ZnO/C nanocomposite: an efficient catalyst for the photocatalytic degradation of Orange G textile dye. *RSC Adv.* **2017**, *7* (48), 30411–30421.
- (62) Abdullah, D.; Gupta, D. C. Exploring the structural, Mechanical, electronic, optical, and thermoelectric properties of Cesium-based double perovskite Cs<sub>2</sub>GeSnX<sub>6</sub> (X= Cl, Br, I) compounds: A DFT study. *Mater. Sci. Semicond. Process.* **2023**, *167*, No. 107813.
- (63) Nassar, M. Y.; Ahmed, I. S.; Samir, I. A novel synthetic route for magnesium aluminate (MgAl<sub>2</sub>O<sub>4</sub>) nanoparticles using sol-gel auto combustion method and their photocatalytic properties. *Spectrochimica Acta Part A: Molecular and Biomolecular Spectroscopy* **2014**, *131*, 329–334.
- (64) Rauf, M. A.; Ashraf, S. S. Fundamental principles and application of heterogeneous photocatalytic degradation of dyes in solution. *Chemical engineering journal* **2009**, *151* (1–3), 10–18.
- (65) Abdelrahman, E. A.; Hegazey, R. M. Facile synthesis of HgO nanoparticles using hydrothermal method for efficient photocatalytic degradation of crystal violet dye under UV and sunlight irradiation. *J. Inorg. Organomet. Polym. Mater.* **2019**, *29*, 346–358.
- (66) Zaman, M. B.; Poolla, R. Morphological tuning of hydrothermally derived visible light active Cu<sub>2</sub>SnS<sub>3</sub> nanostructures and their applications in photocatalytic degradation of reactive industrial dyes. *Opt. Mater.* **2020**, *104*, No. 109853.
- (67) Kush, P.; Deka, S. Anisotropic kesterite Cu<sub>2</sub>ZnSnSe<sub>4</sub> colloidal nanoparticles: Photoelectrical and photocatalytic properties. *Mater. Chem. Phys.* **2015**, *162*, 608–616.
- (68) Zaman, M. B.; Chandel, T.; Poolla, R. Hydrothermal synthesis of Cu<sub>2</sub>FeSnS<sub>4</sub> anisotropic nanoarchitectures: controlled morphology for enhanced photocatalytic performance. *Materials Research Express* **2019**, *6* (7), No. 075058.
- (69) Marien, C. B.; Le Pivert, M.; Azaïs, A.; M'bra, I. C.; Drogui, P.; Dirany, A.; Robert, D. Kinetics and mechanism of Paraquat's degradation: UV-C photolysis vs UV-C photocatalysis with TiO<sub>2</sub>/SiC foams. *Journal of hazardous materials* **2019**, *370*, 164–171.
- (70) Dashtian, K.; Ghaedi, M.; Shirinzadeh, H.; Hajati, S.; Shahbazi, S. Achieving enhanced blue-light-driven photocatalysis using nano-sword-like VO<sub>2</sub>/CuWO<sub>4</sub> type II n-n heterojunction. *Chemical Engineering Journal* **2018**, *339*, 189–203.
- (71) Kumar, K. V.; Porkodi, K.; Rocha, A. F. Langmuir-Hinshelwood kinetics—a theoretical study. *Catal. Commun.* **2008**, *9* (1), 82–84.
- (72) Li, S.; Lin, Q.; Liu, X.; Yang, L.; Ding, J.; Dong, F.; Li, Y.; Irfan, M.; Zhang, P. Fast photocatalytic degradation of dyes using low-power laser-fabricated Cu<sub>2</sub>O–Cu nanocomposites. *RSC Adv.* **2018**, *8* (36), 20277–20286.
- (73) Billany, M. R.; Khatib, K.; Gordon, M.; Sugden, J. K. Alcohols and ethanalamines as hydroxyl radical scavengers. *International journal of pharmaceutics* **1996**, *137* (2), 143–147.